Poster presented at the
IAU Symposium 176 "Stellar Surface Structure"
Vienna, Austria, 1995

Numerical Simulations of Surface Convection in Solar-type Stars

Bernd Freytag[1], Matthias Steffen[2,1], Hans-Günter Ludwig[3]

[1] Institut für Astronomie und Astrophysik der Universität Kiel,
D-24098 Kiel, F.R.G., [supas024@astrophysik.uni-kiel.d400.de]

[2] Astrophysikalisches Institut Potsdam,
D-14473 Potsdam, F.R.G., [MSteffen@aip.de]

[3] Max-Planck-Institut für Astrophysik,
D-85740 Garching, F.R.G., [hgl@mpa-garching.mpg.de]

1 Introduction

The fine scale structure in the magnetically inactive surface regions of the Sun is formed by the time-dependent pattern of granular convection. Similar types of convection are expected on other stars. The surface layers of a convection zone are particularly important and difficult to understand. They play a fundamental role for the photospheric structure (spectroscopy) and determine the total vertical extent of the convection zone (stellar evolution). They are assumed to be the energy sources of solar oscillations. Also, these layers produce acoustic energy and have mechanical interaction with magnetic fields to heat the outer regions of a star (chromosphere, corona).

The difficulties arise from the non-linear (magneto-) radiation hydrodynamics which produce a complex turbulent flow in a highly stratified medium. Usually local mixing-length theory (MLT) is used to model the effect of convection on the mean stratification and its free parameter is calibrated e.g. by evolutionary calculations. But especially in the surface layers the mixing-length approach becomes questionable and helioseismology reveals its shortcomings (Rosenthal et al. 1995).

A way to gain insight into the complex dynamics of stellar surface convection is the integration of the basic equation with the help of powerful computers, which has been done successfully for the Sun (see e.g. Nordlund 1985) and some solar-type stars (Nordlund & Dravins 1990).

2 Numerical simulations

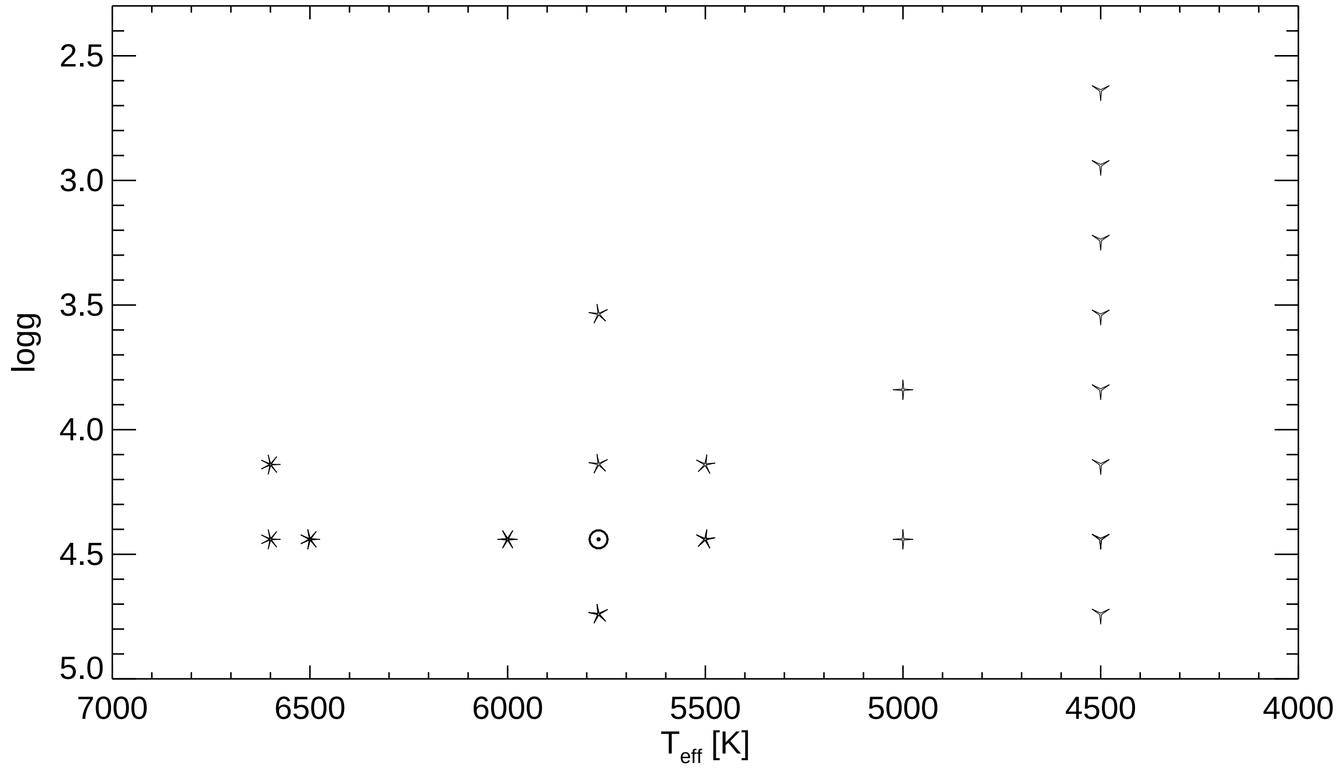

Figure 1: Grid of numerical models in the $T_{\rm eff}/\log g$ plane (g in cgs-units).

In contrast to Nordlunds 3D simulations in this study a 2D approximation is used. This allows a finer grid which is particularly important to resolve the sharp temperature rise just below the visible stellar surface. It permits longer runs to account for the long thermal relaxation times and makes it possible to produce a number of models with different physical and/or numerical parameters with reasonable computational effort.

Based on 2D numerical radiation hydrodynamics calculations of time-dependent compressible convection, a variety of stellar surface convection zones has been studied. The equation of state accounts for the formation of H_2, H, H^+, He, He^+, He^{++} and a neutral metal. The non-local equation of radiative energy transport is solved along a number of representative rays, assuming LTE. Grey or simple frequency-dependent opacities are used (for details see Ludwig et al. 1994)

The lateral boundary conditions are periodic. The top is transmittend for sound waves. The lower boundary condition allows the free in- and outflow of material. Here the inward mass flux is adjusted to keep the mass inside the model constant and the entropy of the inflowing material is regulated to keep the total radiative flux at the top equal to $\sigma T_{\rm eff}^4$.

The list of models with open lower boundary so far covers (near) main-sequence stars with $4\,500\,\mathrm{K} \leq T_{\rm eff} \leq 6\,600\,\mathrm{K}$, $2.64 \leq \log g \leq 4.74$ (see Fig. 1). Additionally there are models of shallow convection zones (main-sequence A-type stars and cool DA white dwarfs) which are completely included in the computational volume and allow especially the investigation of overshoot below the convection zone.

3 Results

3.1 Dynamics of the convective flow

Typical examples of flow patterns are presented in Fig. 2 to 5. The models comprise the photosphere and the upper part of the convection zone. The velocity field is indicated by short pseudo-streamlines followed over $t_{\rm int}$ for an instantaneous velocity field. Contour lines indicate the temperature T (upper panel), the Mach number Ma (center), and the specific entropy s (lower panel). Small tick marks at the top and the right show the positions of the computational grid points (142×71). Four columns at the right show some horizontally averaged quantities: the sign of the vertical entropy gradient, the sign of the vertical enthalpy flux, the natural logarithm of the mean pressure, and the logarithm of the optical depth. A positive entropy gradient defines a convectively stable region and a negative one an unstable zone. The origin of the height scale on the left corresponds to the layer with $\log \tau = 0$. The height z is counted upward. The lower boundary allows the free in- and outflow of material. The top is open for waves. The lateral boundary conditions are periodic. The chemical composition is solar. Grey opacities are used.

The turbulent dynamics are governed by fast, narrow, cool downflows extending from the stellar surface into great depth. They are surrounded by broad hotter regions with small upward velocities. New downdrafts are created in quiet regions by convective instability (Fig. 2, top panel, on the left). They are advected horizontally until they merge with others, thereby producing deep reaching plumes and strong emission of sound waves.

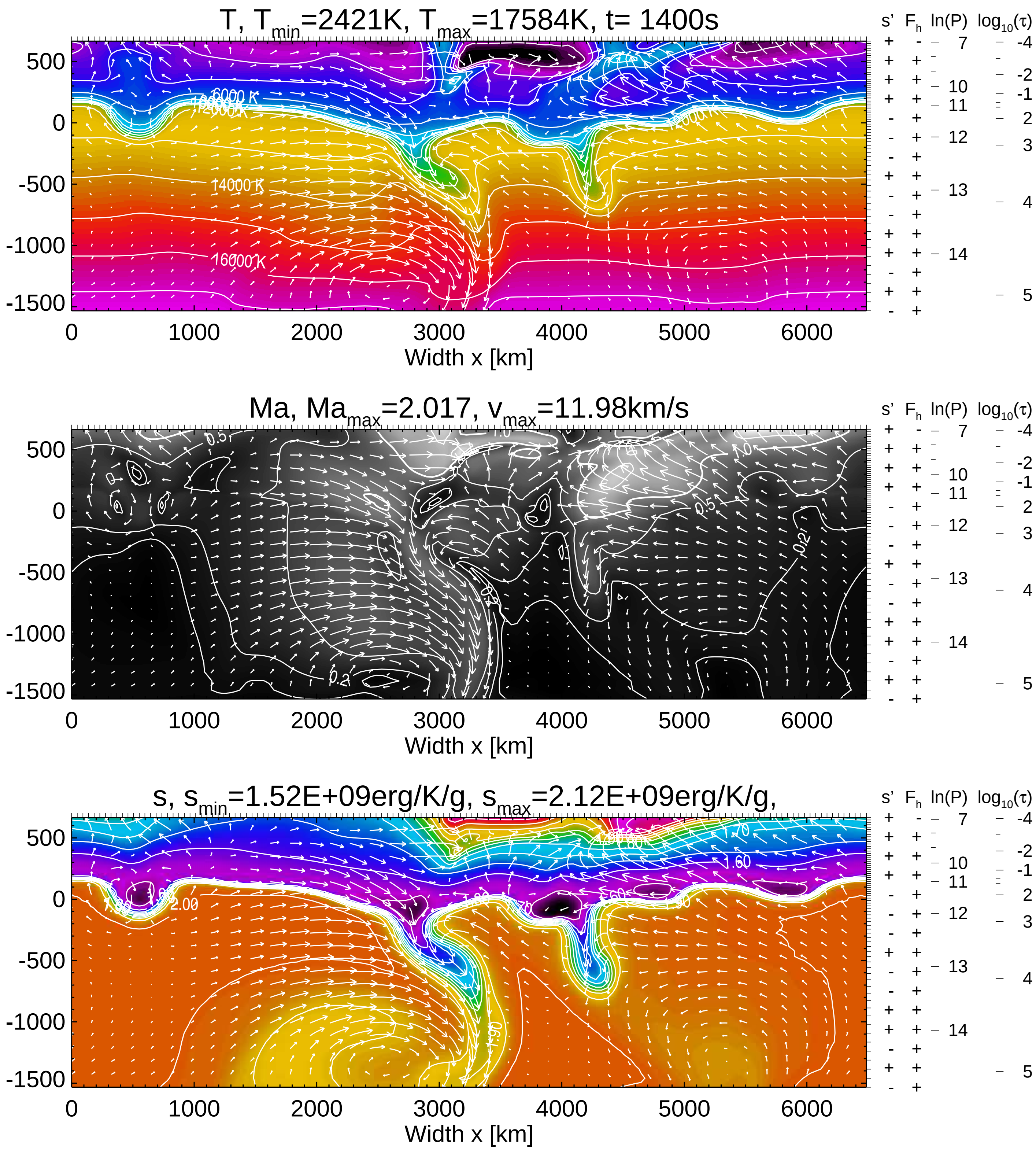

Figure 2: Snapshot of a main-sequence F star model (GT65g44N2) with $T_{\rm eff} = 6\,500\,$K, $\log g = 4.44$, $t_{\rm int} = 25$ s, 142×71 grid points. For a selected instant of time the temperature T, the Mach number Ma, and the specific entropy s are displayed as color and contour plots together with pseudo-streamlines for the velocity.

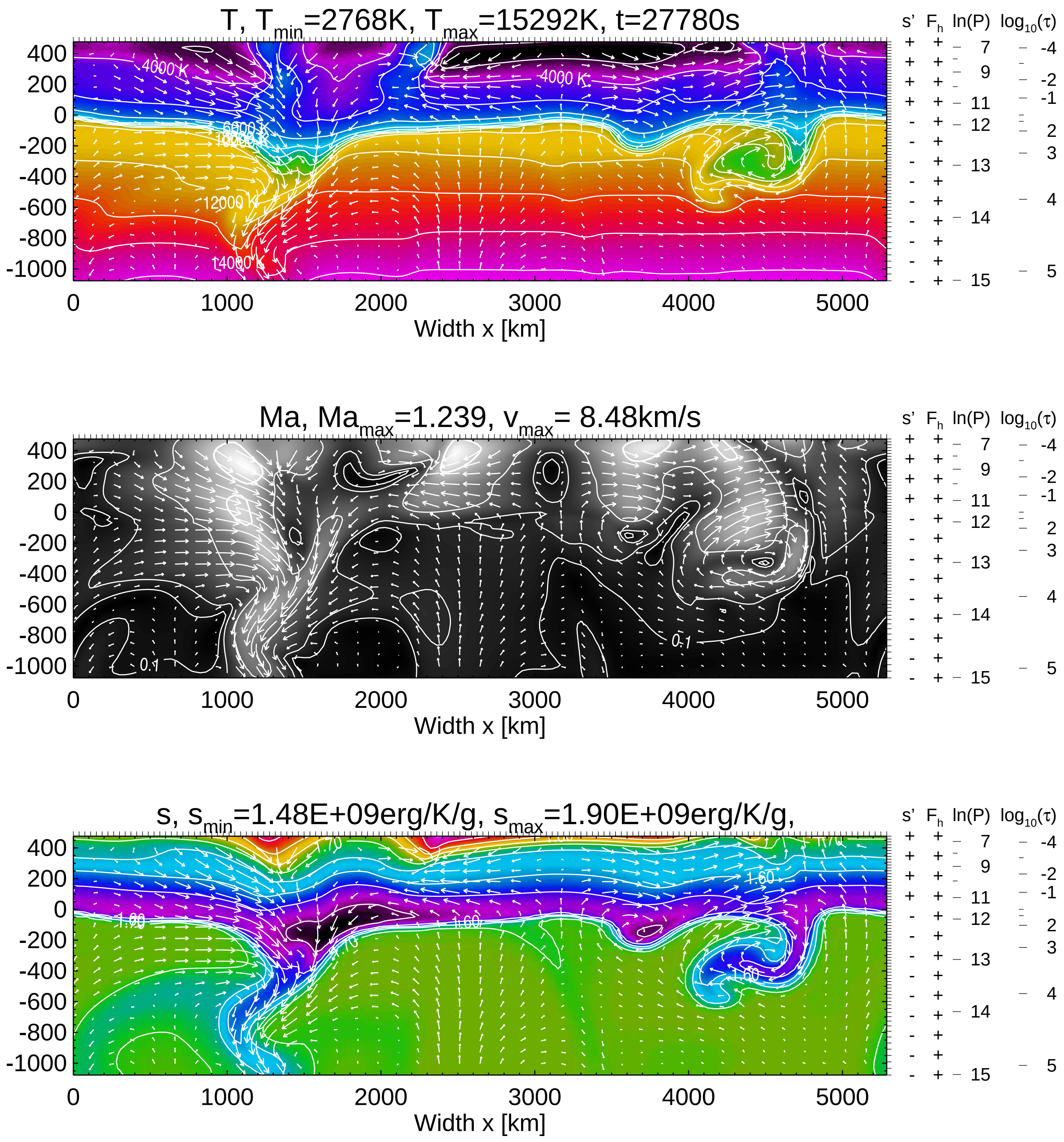

Figure 3: Snapshot: G star model (GT57g44N1) with $T_{\rm eff}$ = 5 700 K, $\log g$ = 4.44 (Sun), $t_{\rm int}$ = 25 s, 142 × 71 grid points.

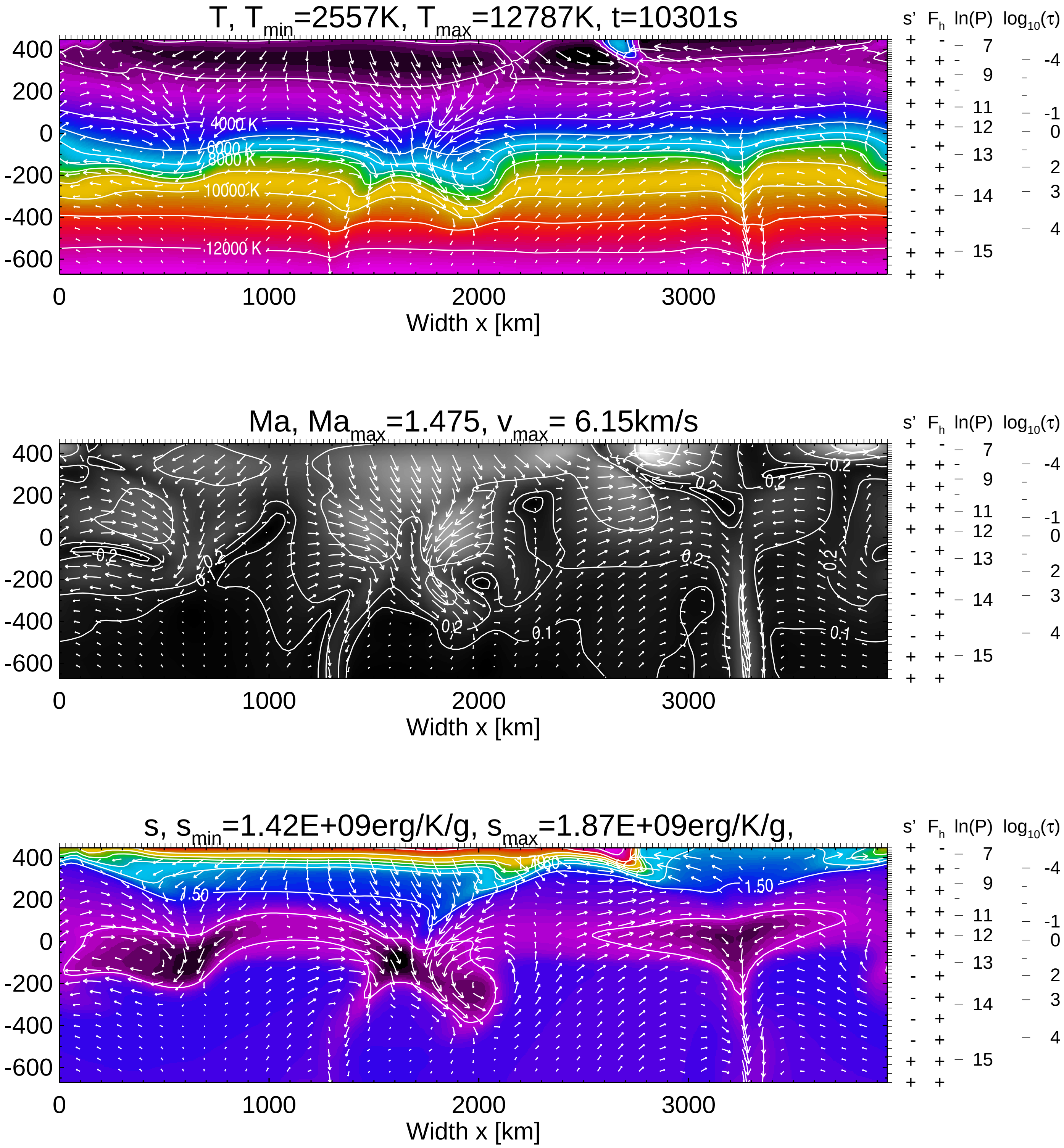

Figure 4: Snapshot: K star model (GT45g44N1) with $T_{\rm eff} = 4\,500\,{\rm K}$, $\log g = 4.44$, $t_{\rm int} = 25$ s, 142×71 grid points.

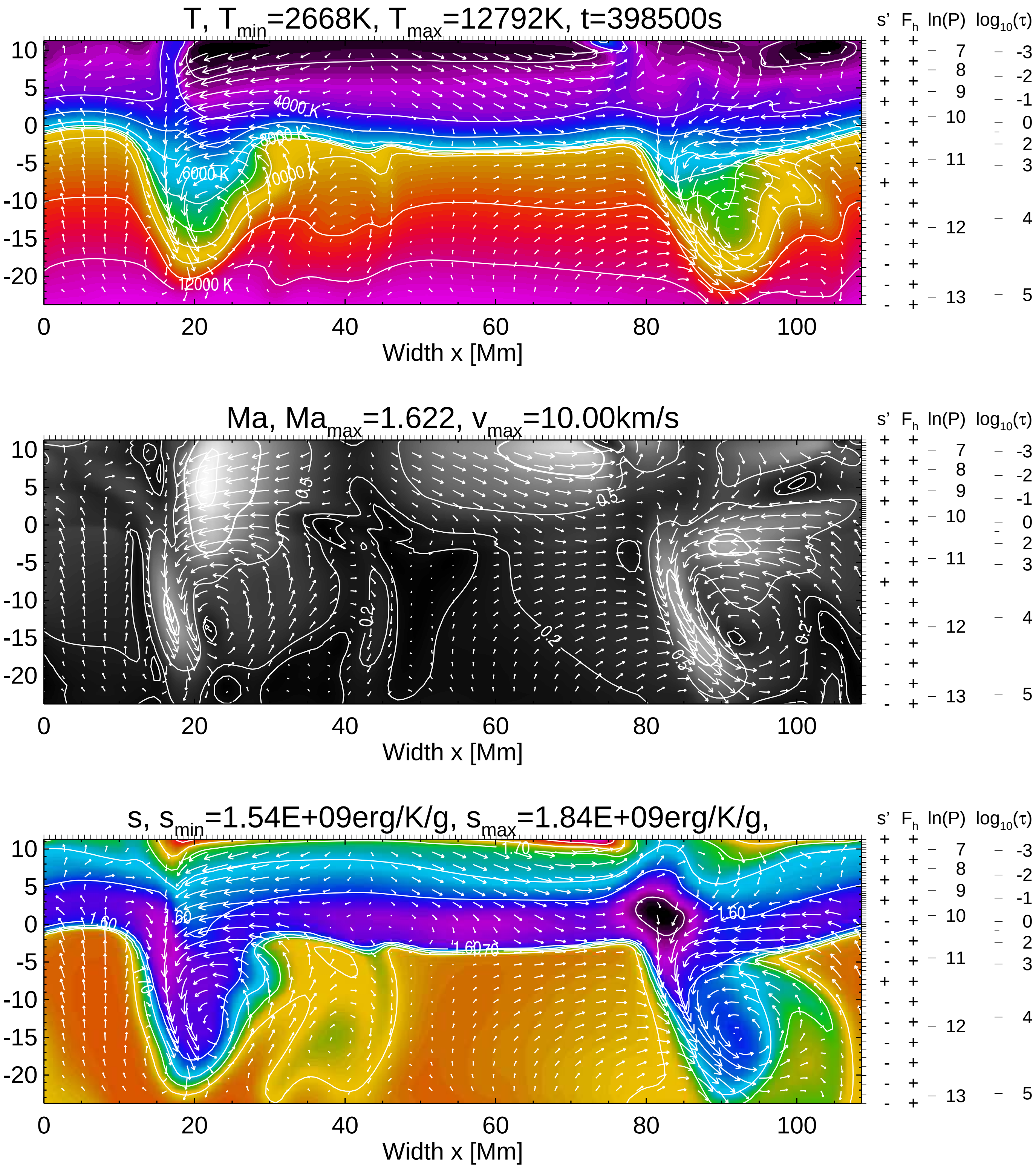

Figure 5: Snapshot: K star model (GT45g29N1) with $T_{\rm eff} = 4\,500\,$K, $\log g = 2.94$, $t_{\rm int} = 500$ s, 142×71 grid points. Note the significantly larger scale than in the main-sequence models.

3.2 Effects of surface convection on the stellar interior

The structural changes in the surface of the convection zone with effective temperature for solar-type stars are visible in the main-sequence models with $T_{\rm eff} = 6\,500\,{\rm K}$ and $T_{\rm eff} = 4\,500\,{\rm K}$ ($\log g = 4.44$) in Fig. 2 and 4, respectively.

Towards lower effective temperatures convection has to transport less flux at higher densities. Thus smaller temperature fluctuations and vertical velocities are sufficient. The largest Mach numbers are found in the photosphere. They are in the hotter model generally slightly higher than in the cooler (Fig. 2 and 4, center panel).

Conspicuous is the different size of the temperature rise with depth directly beneath the visible surface. In the hotter model there is a sharp edge where the temperature increases by $5\,000\,{\rm K}$ across a few grid points. It is caused by a sharp peak in the opacity as can be deduced by the distortion of the scale of the mean optical depth on the right of Fig. 2. The temperature field in the cooler model is comparatively smooth (Fig. 4).

Together with the temperature the specific entropy shows a sharp rise beneath the photosphere (see Fig. 2 to 5, lower panel). But underneath this boundary layer the entropy fluctuations are remarkably small. They are essentially confined to the inside and neighborhood of the cool downdrafts. The broad upstream regions show an entropy plateau. The steepness and size of the step depend on effective temperature and gravity (see Fig. 6). Assuming that the value of the entropy plateau can be directly identified with the entropy of the deep, adiabatic convective layers, it is possible to calculate MLT models with a corresponding entropy of the deep adiabat and to derive in this way an effective mixing-length parameter α (Steffen 1993). Its variation with effective temperature and gravity is demonstrated in Fig. 7. In the main-sequence phase the effective α for the Sun is a constant close to 1.70. But it increases during the evolution towards the red giant branch (Ludwig et al. 1995).

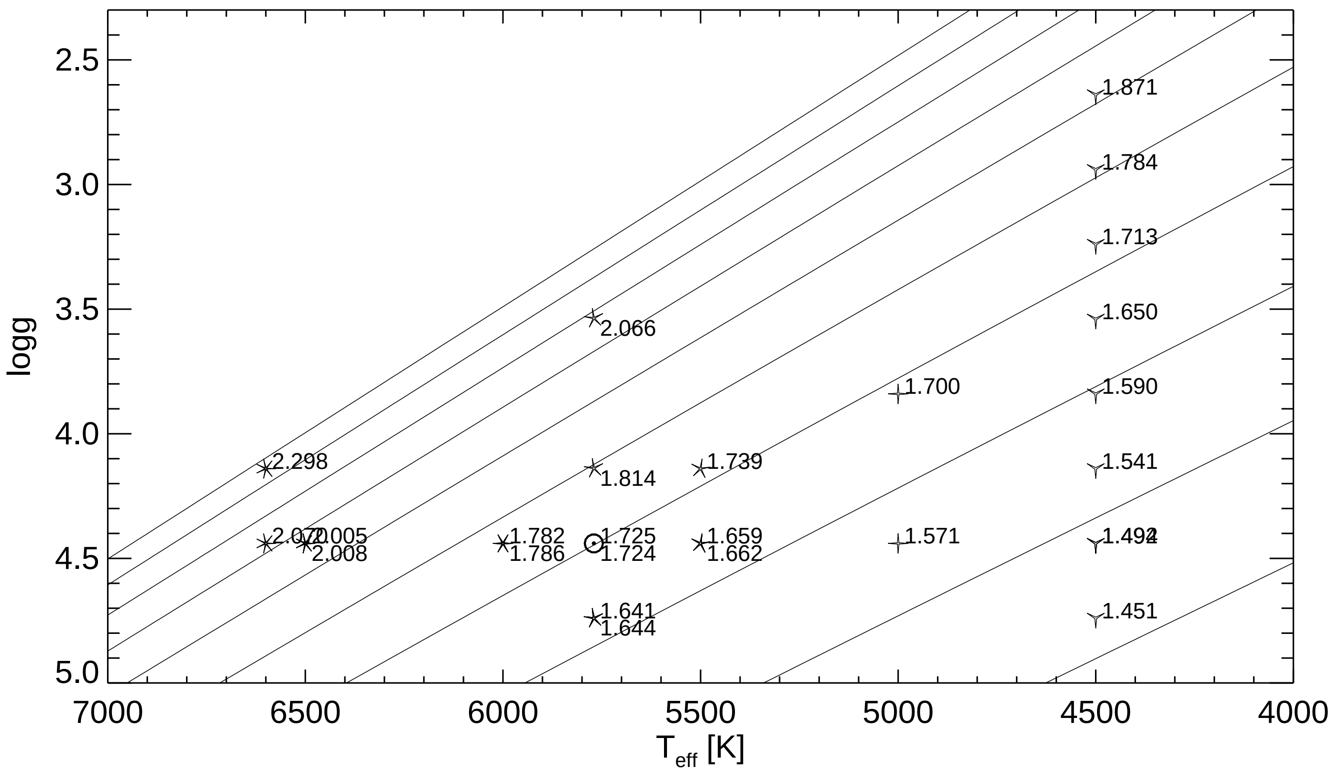

Figure 6: Entropy in the deep interior in the $T_{\rm eff}/\log g$ plane. Each symbol indicates the location of one (or more) models. The number on the right of each symbol is the value of the entropy plateau (s^* in 10^9erg/K/g), which corresponds to the value of the adiabat in the deep convective layers. A smooth function has been fitted to the (small) sample of points and boldly applied to other values in the parameter space. The run of its contour lines (in steps of 10^8erg/K/g) should only guide the eyes clarify that the entropy s^* grows with increasing effective temperature and decreasing gravity.

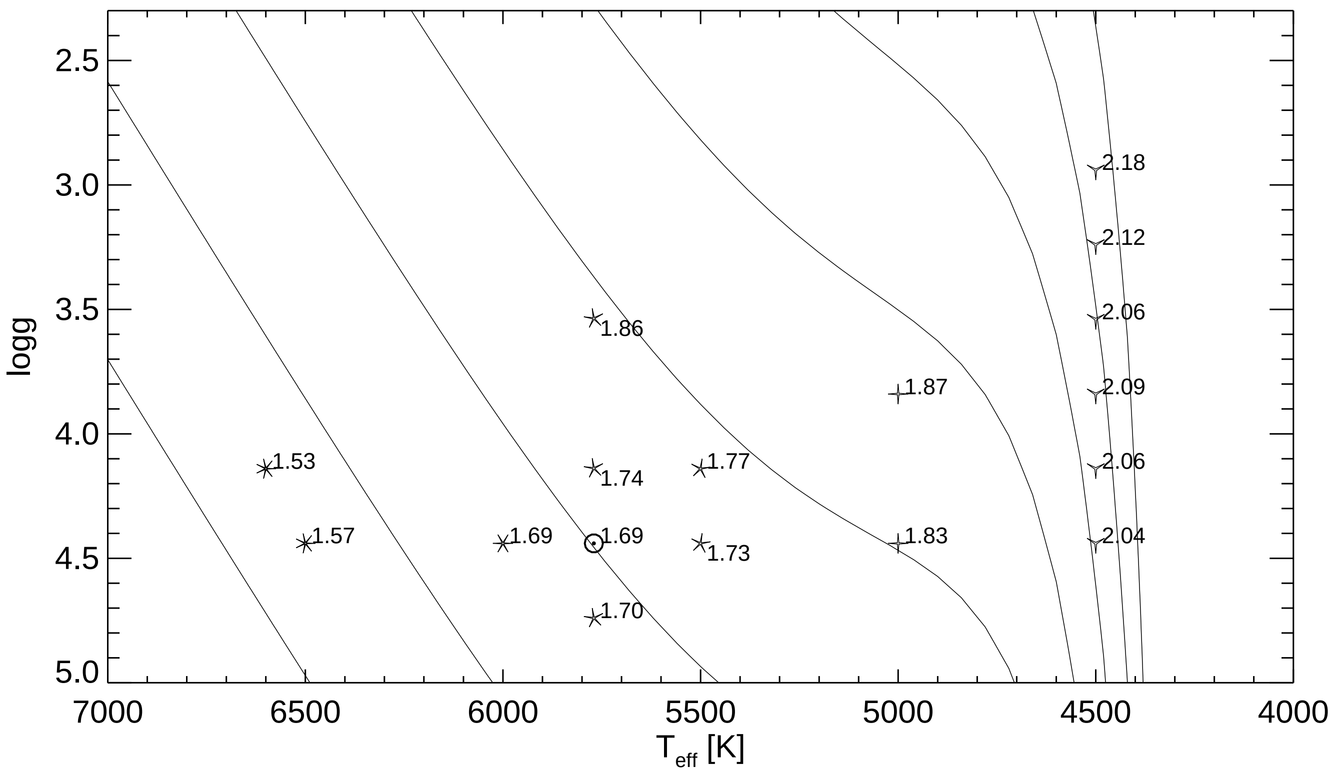

Figure 7: Mixing-length parameter α in the $T_{\rm eff}/\log g$ plane. The number on the right of each symbol is the effective α, derived from the entropy values in Fig. 6. The contour lines are in steps of 0.1.

3.3 Effects of surface convection on the outer atmosphere

One aim of this study is to determine the amount a acoustic energy produced by convection and to determine its temperature and gravity dependence. The acoustic flux can be computed directly from the numerical models (Steffen 1994). The maximum of the rms-value of the vertical velocity increases with increasing effective temperature and decreasing gravity (Fig. 8) in a similar way as the entropy of the instreaming material (Fig. 6).

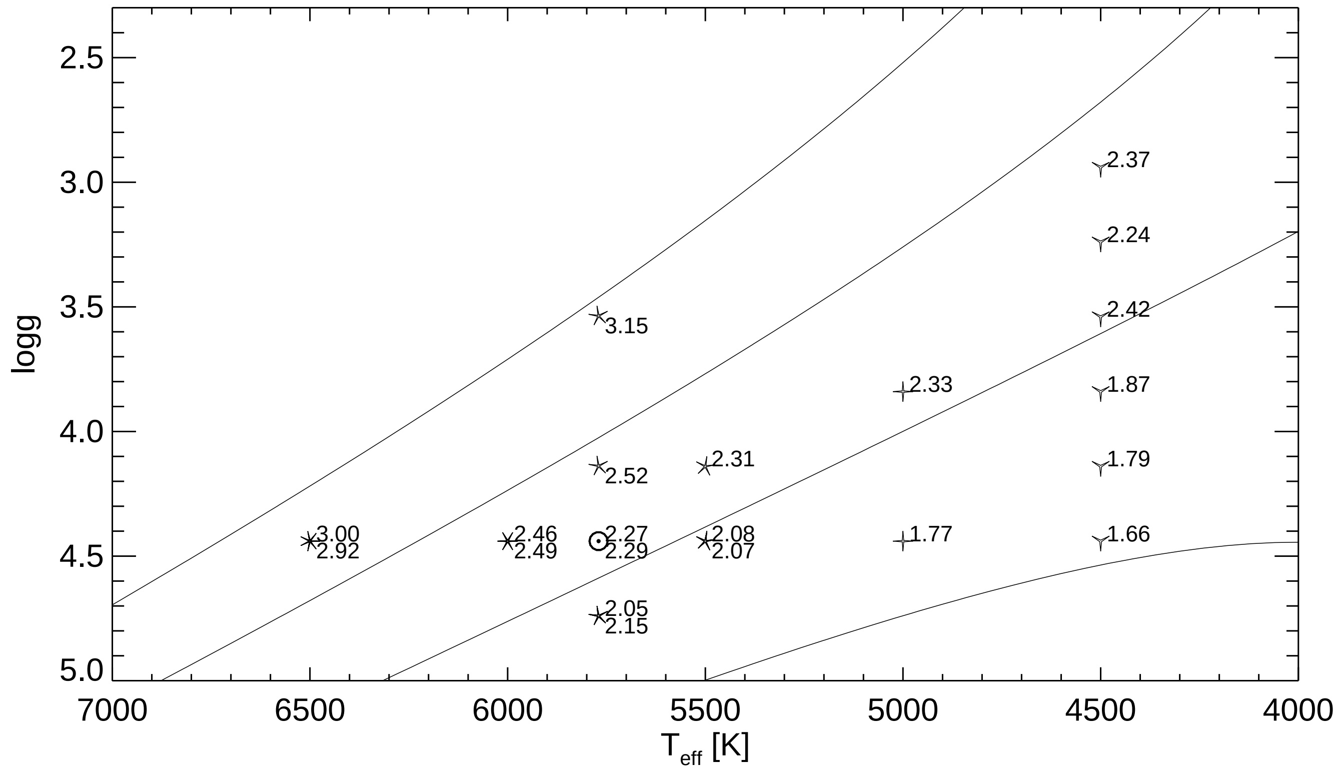

Figure 8: Maximum of the rms-value of the vertical velocity in the $T_{\rm eff}/\log g$ plane (in km/s).

But the acoustic flux shows stronger fluctuations from model to model and no clear systematic trend with $T_{\rm eff}$ or $\log g$. At $\tau = 0.01$ it has for all models a typical size of $1\%\,\sigma T_{\rm eff}^4$.

Thus there is so far no indication that a drastic change in the convective sound production might be responsible (in some way) for the disappearance of coronae at low effective temperatures (Haisch et al. 1991).

References

Haisch B., Schmitt J.H.M.M., Rosso C., 1991, ApJL 383, 15-18

Ludwig H.-G., Freytag B., Steffen M., Wagenhuber J., 1995, in "Stellar Evolution: What Should Be Done", 32nd Liège Int. Astroph. Col., 1995

Ludwig H.-G., Jordan S., Steffen M., 1994, A&A 284, 105

Nordlund Å., 1985, Sol. Phys. 100, 209

Nordlund Å., Dravins D., 1990, A&A 228, 155

Rosenthal C.S., Christensen-Dalsgaard J., Nordlund Å., Trampedach R., 1995, Proc. 4th SOHO Workshop: Helioseismology, eds. V. Domingo et al., ESA SP-376, ESTEC, Noordwijk

Rosenthal C.S., Christensen-Dalsgaard J., Houdek G., Monteiro M.J.P.F.G, Nordlund Å., Trampedach R., 1995, ibid.

Steffen M., 1993, in "Inside the stars", IAU Colloquium 137, eds. W. Weiss, A. Baglin, Astron. Soc. Pacif. Coonf. Series Vol. 40, p. 300

Steffen M., 1994, in "Solar Magnetic Fields", eds. M. Sch"ussler, W. Schmidt, Cambridge University Press, p. 294-297